Stochastic approach to simulation of lattice vibrations in strongly anharmonic crystals: Anomalous frequency dependence of the dynamic structure factor

Yu. N. Gornostyrev and M. I. Katsnelson
Institute of Metal Physics, Ural Division of Russian Academy of Sciences, 620219, Ekaterinburg, Russia

A. V. Trefilov
Russian Scientific Centre ''Kurchatov Institute,'' 123182, Moscow, Russia

S. V. Tret'jakov*
Institute of Metal Physics, Ural Division of Russian Academy of Sciences, 620219, Ekaterinburg, Russia
(Received 15 September 1995; revised manuscript received 23 April 1996)

A simple model describing the dynamics of a collective strongly anharmonic mode embedded in a thermostat is investigated by numerical integration of the Langevin equation using methods with strong and weak convergences. We apply *ab initio* potentials with several wells describing some types of such modes in the bcc phase of Zr. The results obtained demonstrate a number of peculiarities of lattice vibrations, which do not keep within the limits of the conventional phonon picture. In particular, an analysis of the results allows one to explain some unusual features of the lattice dynamics of Ti and Zr and their alloys (for example, symmetrically forbidden splitting of phonon branches, central peak). [S0163-1829(96)07929-5]

I. INTRODUCTION

Recent inelastic neutron scattering experiments in high temperature bcc phases of Ti, Zr, Hf, La, and Sc (see, Ref. 1 and references therein) have again attracted attention to the old and still unsolved problem of the description of lattice dynamics in the presence of strong anharmonicity, frequently arising near structural instabilities. A number of unusual phenomena in alloys $Zr_{1-x}Nb_x$, such as the central peak in neutron scattering, symmetrically forbidden splitting of phonon branches, and anomalies of quasielastic scattering of Mössbauer radiation, were discovered long ago in Refs. 2,3. As was recently shown (see, Ref. 1), the transversal phonon branches in the high-temperature β (bcc) phase of the abovementioned metals along the $\langle 110\rangle$ and $\langle 112\rangle$ directions, related to the β-α (hcp) and β-ω transitions (see Sec. II), were poorly determined, and a broadband distribution of scattered neutrons in energy was observed instead of the central peak which was typical for Ti- and Zr-based alloys.[2]

In general, the anharmonic effects for most vibration modes in all crystals can be considered, based on perturbation theory with respect to the adiabatic parameter, as the effects of weak nonideality of the phonon gas. Indeed, due to the Lindemann criterion, the inequality $\overline{u^2} \simeq 0.01a^2 \ll a^2$ is valid at $T = T_m$ (a is a lattice constant, and T_m is the melting temperature), where $\overline{u^2}$ is the mean square of atomic displacement. If anharmonicities are very strong in a considerably large part of the Brillouin zone at $T < T_m$, this criterion cannot certainly be fulfilled. However, anharmonicity of the potential energy V can be very strong for some distinguishable vibration modes in metals near structural instability, resulting in several stable equilibrium positions (see, for example, Refs. 4,5). This is confirmed by direct calculations using the frozen phonon method for different deformations of Zr (Refs. 6 and 7) and Ba (Ref. 8) lattices in the bcc (β)-phase. Multiwell potentials appear to be typical for crystals undergoing structural transitions, in particular martensitic transformations in metals.[9]

One could think that the effects of strong anharmonicity lead only to a renormalization of the phonon frequency and an increase of phonon damping (for example, in the spirit of the self-consistent phonon approach[10]). For instance, in the Ref. 1 experimental data which demonstrated the broadband energy distribution of inelastic neutron scattering were interpreted in the limits of the traditional phonon picture, although the width of the phonon peak was comparable with its frequency.

Starting from the pioneer paper by Krumhansl and Schrieffer[4] the soliton (more exactly, kink) theory of lattice dynamics in strong anharmonic crystals has been intensively developed.[11,12,9] In particular, this theory allowed us to explain the presence of the central peak qualitatively.[4] However, the central peak is not the unique unusual feature observed in the experiments.[1] Another important peculiarity in the inelastic scattering cross section measured in Ref. 1 is the broadband distribution in energy. A considerable part of the spectral density was observed in the frequency region below the usual phonon frequencies but above the central peak. A qualitative explanation of this peculiar phenomenon is the main aim of the present paper.

To clarify this question, it appears to be natural to start from the simplest model of one distinguishable collective mode which is embedded in a thermostat of all other excitations. We hope that despite the model under consideration being oversimplified, it includes, nevertheless, the main features important for real systems. The power spectral density (PSD) of a generalized coordinate determining the collective mode is an analog of the dynamic structure factor which is measured in inelastic neutron scattering experiments. If the PSD as a function of frequency is characterized by a single clearly observed maximum at $\omega = \omega_0 \neq 0$, it is natural to con-

sider ω_0 as a phonon frequency which can depend on temperature in general case, and the width of the peak is associated with phonon damping. If the PSD as a function of ω has several peaks or is monotonous, then no specific energy of excitation corresponds to the given transferred momentum during inelastic neutron scattering. In this case we shall speak about the nonphonon picture of lattice dynamics.

The approximations made are discussed in Sec. II and the formulation of the model is given. In Sec. III numerical methods are described in detail, in Sec. IV the results obtained are presented and in Sec. V we discuss the results of simulation.

Some preliminary results were previously published in Ref. 13.

II. APPROXIMATIONS AND FORMULATION OF THE MODEL

In Refs. 4,14 the following model of a strongly anharmonic crystal was considered. The on-site potential of each atom (displacing ion in terms of Ref. 4) is bistable and different atoms are connected by ''springs.'' A single atom at a constant temperature jumps between two wells, the average displacement being equal to zero. The inclusion of atom interaction results in either a phase transition (if the dimension of the crystal is greater than 1) or a short-range order in the one-dimensional (1D) case.[4] Bearing in mind the application of the model to structural phase transitions of displacement type rather than order-disorder type,[15] we shall consider the anharmonic potential for a *collective vibration mode*. If only a *single* mode is chosen, we, of course, cannot describe the phase transition itself (just as one would retain only one atom in the approach of Refs. 4,14). But, in our opinion, this simple model describes the lattice dynamics of strongly anharmonic crystals above the transition temperature qualitatively correctly, since in this case the vibration modes are quasi-independent. Just that very case is realized in the experiments.[1] To build a more realistic description of the lattice dynamics of strongly anharmonic crystals one must solve nonlinear equations for interacting *atoms*, resulting in the formation of inhomogenous domains in **r** space similar to nucleations of a new phase, or consider the model including *a set of* coupling vibration modes, i.e., take into account the spatial dispersion. In this sense the investigated model is a rough idealization which, as we hope, catches the principal features of the considered phenomenon.

To explain the notion of a collective variable which is the key for the formulation of our model, it is convenient to choose, as an example, the β-ω transition. The ω phase arises from the β phase (bcc) as a result of merging of atomic planes {111} with period tripling (see Fig. 1). Let us then describe a displacement of these planes from equilibrium positions along the direction $\langle 111 \rangle$ by introducing some generalized coordinate X in such a way that the total energy of a crystal per atom $V(X)$ has minima at points $X=0$, if the β phase is stable with respect to small perturbations, and $X=d/2$ (d is the distance between planes), if the ω phase is stable. Therefore, the potential energy $V(X)$ is a multiwell function near the β-ω phase transition line and, hence, is strongly anharmonic.

More exactly, consider a displacement field depending on

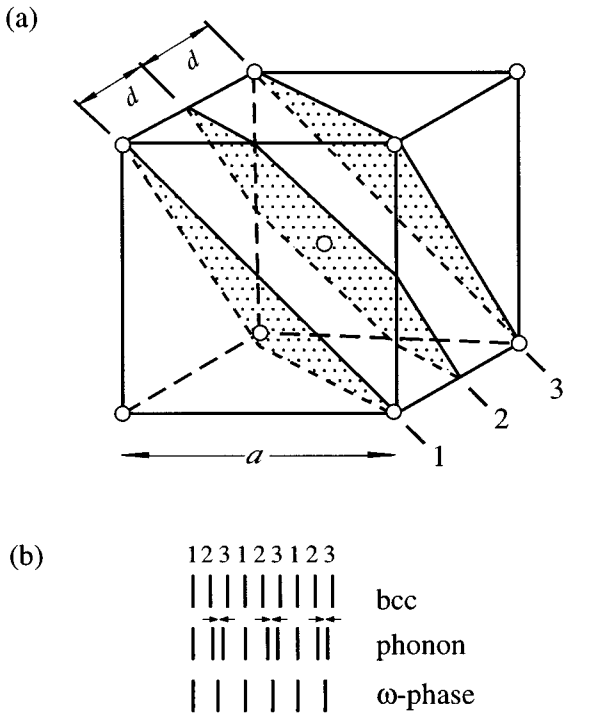

FIG. 1. (a) bcc lattice and three neighboring (111) planes; (b) spacing of the planes for bcc and ω-phase and plane vibrations corresponding to the longitudinal phonon (2/3,2/3,2/3).

spatial coordinates **r** and time t in the form

$$\mathbf{u}(\mathbf{r},t)=\mathbf{e}X(\mathbf{r},t)\cos(\mathbf{Q}\cdot\mathbf{r}), \tag{1}$$

where $\mathbf{e}=(1/\sqrt{3})(1,1,1)$ is a polarization vector, $\mathbf{Q}=(4\pi/3a)(1,1,1)$ is the wave vector corresponding to the mode which transforms the β phase to the ω phase, and a is a lattice constant $[d=(\sqrt{3}/2)a]$. Let us suppose that the anharmonic effects are strong only in a small region of **q** space near the point **Q** and the function $X(\mathbf{r},t)$ contains Fourier components (with respect to **r**) only from this area. Therefore $X(\mathbf{r},t)$ is a slowly varying function of **r** compared to the lattice constant a. We start from the equations of motion for the generalized coordinate $X(\mathbf{r},t)$ which take into account the anharmonicity of the potential $V(X)$, the interaction with all other vibration modes of the crystal being simulated by the inclusion of a thermostat into the equations of motion. Later we shall neglect the effects of spatial dispersion, i.e., the dependence of $X(\mathbf{r},t)$ on the coordinate **r**. A qualitative discussion of some effects implied from the spatial dispersion one can be seen in Refs. 5,16.

Neglect of the spatial dispersion, which is based on the assumption that anharmonic effects are strong only in a small neighborhood of the point $\mathbf{q}=\mathbf{Q}$ in reciprocal space, may be justified to some extent. In fact, as we have discussed in the Introduction, due to the Lindemann criterion, anharmonicities cannot be very strong in a considerably large part of the Brillouin zone even at melting temperature. In some situations, for example, for the bcc-hcp phase transition, it is necessary to introduce two collective variables, describing the

transformation from one crystal structure to another.[8] In the present paper we shall confine ourselves to the simplest case of one variable.

Based on the assumptions mentioned above, a detailed formulation of the original equations is given. Consider the case of a harmonic crystal. Then there is the well-known canonical transformation to the normal coordinates which determine the vibration modes (phonons) of the given system. Let all these modes, except one distinguishable mode, be in thermal equilibrium at the initial instant of time. As Bogoliubov showed,[17] while switching on the interaction of the distinguishable mode with others it is also thermalized, this process being described by the Fokker-Planck equation (FPE). The last one is known to be equivalent to the Langevin equation (see, for example, Ref. 18) in which the interaction of the distinguishable mode with all others is simulated by including a viscous friction and a random force of the white noise type. A detailed discussion of the applicability of the Langevin equation approach to systems with anharmonic potentials was given in Ref. 19 in connection with a consideration of the dynamics of the Josephson contacts. In that paper both quantum and classical regimes have been discussed. We restrict ourselves to the classical limit of not too high characteristic frequencies $\hbar\omega \ll T$ (T is a temperature), where the white noise approximation holds.

Thus, the dynamics of the variable $X(t)$ is described by the Langevin equation

$$m\frac{d^2X}{dt^2} = -\frac{dV(X)}{dX} - \Gamma\frac{dX}{dt} + F(t), \tag{2}$$

where m is the atom mass, Γ is the damping of small vibrations with $\mathbf{q}=\mathbf{Q}$, and $F(t)$ is the Gaussian white noise,

$$\langle F(t)F(t')\rangle = 2\tilde{T}\Gamma\,\delta(t-t'). \tag{3}$$

The coefficient in relation (3) is such that Eq. (2) describes the relaxation of the distribution function $P(X,\tilde{v},t)=\langle \delta(X-X(t))\delta(\tilde{v}-\tilde{v}(t))\rangle$ to the stationary Boltzman distribution

$$P_{\mathrm{st}}(X,\tilde{v},t=\infty) = \exp\{-[m\tilde{v}_{\mathrm{st}}^2/2 + V(X_{\mathrm{st}})]/\tilde{T}\},$$

with the temperature $\tilde{T}$ and stationary values of the coordinate X_{st} and the velocity $\tilde{v}_{\mathrm{st}}=\sqrt{\tilde{T}/m}$.[18]

In principle, the function $V(X)$ can be calculated, for example, by the frozen phonon method[6–8] as a variation of the total energy of crystal per atom for the crystal deformation corresponding to the given mode [see Eq. (1)]. In particular, specifying the deformation of the form (1) in the model of pair central forces with the potential $\phi(\mathbf{R})$ we obtain in the harmonic approximation

$$V(X) = \frac{1}{2N}\sum_{\mathbf{R}\mathbf{R}'}\phi(|\mathbf{R}-\mathbf{R}'+\mathbf{u}(\mathbf{R})-\mathbf{u}(\mathbf{R}')|)$$

$$= \frac{X^2}{4N}\sum_{\mathbf{R}\mathbf{R}'} e_\alpha e_\beta \frac{\partial^2\phi(|\mathbf{R}-\mathbf{R}'|)}{\partial R_\alpha \partial R_\beta}[\cos(\mathbf{Q}\cdot\mathbf{R}) - \cos(\mathbf{Q}\cdot\mathbf{R}')]^2 = \frac{\omega^2(\mathbf{Q})X^2}{2}, \tag{4}$$

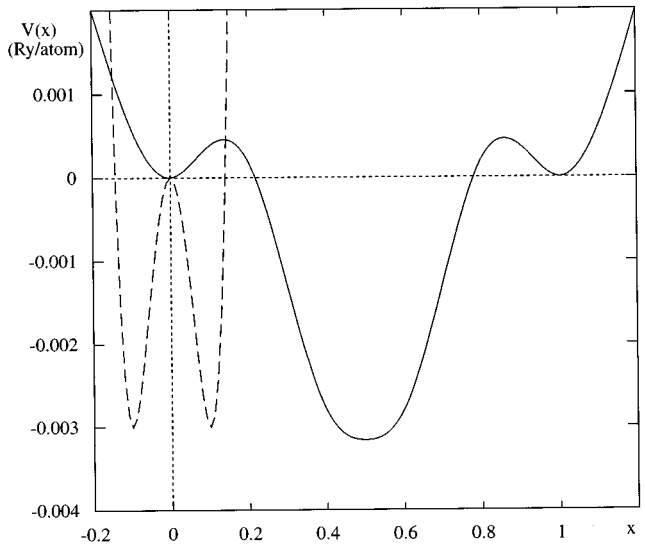

FIG. 2. The total energy $V(x)$ as a function of displacements corresponding to the longitudinal phonon with $\mathbf{q}=(2\pi/a)(2/3,2/3,2/3)$ (solid line) (Ref. 6) and the transversal phonon with $\mathbf{q}=(2\pi/a)(1/2,1/2,0)$ (dashed line) (Ref. 7); x is measured in units of the corresponding interplane distances.

where $\omega^2(\mathbf{Q})$ is the phonon frequency with wave vector $\mathbf{Q}$ and polarization vector $\mathbf{e}$ (see, for example, Ref. 16).

Thus, the Langevin equation is used as a stochastic approach to the molecular dynamics problem at constant temperature, which is supported by the balance between the friction and the random force $F(t)$ in (2). Such an approach has been described in Ref. 20. However, only recently have numerical methods for solution of systems of stochastic differential equations (SDE's), efficient in a computing sense and mathematically justified, been constructed,[21,22] the Langevin equation being a special case of a SDE.

Another more ordinary method of the inclusion of temperature into the molecular dynamics of physical systems is the Nosé-Hoover thermostat.[23] In this approach thermalization is achieved by interaction of the investigated system with a certain additional degree of freedom which is chosen in a special form. However, this approach, in contrast to the Langevin equation, has turned out to be nonapplicable for systems with a small number of degrees of freedom. For example, numerical calculation[24] did not allow us to reproduce the stationary Boltzmann distribution for the one-dimensional harmonic oscillator being in thermal contact with the heat bath.

The functions $V(X)$, which were obtained as a result of calculations for β-Zr and corresponded to the displacement of atoms along the $\langle 111\rangle$ direction with $\mathbf{q}=\mathbf{Q}$ (β-ω transition) (Ref. 6) and along the $\langle 1\bar{1}0\rangle$ direction with $\mathbf{q}=(2\pi/a)(\frac{1}{2},\frac{1}{2},0)$ (one of the variables ''taking part'' in the β-α (hcp) transition) are chosen as an example of strong anharmonic potentials (see Fig. 2). In the first case the deep and shallow minima correspond to the ω and β phases showing the instability of β-Zr at $T=0$ with respect to the β-ω transition [the potential energy $V(X)$ is symmetrically continued relatively to the minimum]. In the second case the maximum of $V(X)$ at $X=0$ points to an instability of β-Zr at $T=0$ with respect to the β-α transition. The problem of the

lattice dynamics simulation with such potentials is a model one since in Refs. 1 and 2 the β phase stabilized by entropy contributions at high temperatures was substantively experimentally investigated, but rigorous calculations, which take into account these contributions and are similar to that in Refs. 6,8, are not yet possible. However, one can consider that such features of $V(X)$, as the presence of several wells and the smallness of the corresponding barriers heights, are typical for metals and alloys near martensitic transformations.

At last it is convenient to go over to natural dimensionless variables $x=X/d$, $\gamma=\Gamma/\omega_0$, $U(x)=V(x)/\alpha d^2$, $T=\widetilde{T}/\alpha d^2$, and $\tau=t\omega_0$, and $f(\tau)=F(t)/md\omega_0^2$, where

$$\alpha=\frac{1}{d^2}\left.\frac{\partial^2 V(x)}{\partial x^2}\right|_{x=x_{\min}},$$

and $\omega_0=\sqrt{\alpha/m}$, for the three-well potential $x_{\min}$ means the coordinate of a shallow well. Then Eqs. (2) and (3) take the form

$$\frac{d^2x}{d\tau^2}=-\frac{dU(x)}{dx}-\gamma\frac{dx}{d\tau}+f(\tau), \tag{5}$$

$$\langle f(\tau)f(\tau')\rangle=2T\gamma\delta(\tau-\tau'). \tag{6}$$

In conclusion, we shall rewrite the Langevin equations (5) and (6) in the form adopted in the theory of SDE's,

$$dx=v\,d\tau,$$

$$dv=[-U'(x)-\gamma v]d\tau+\sigma dW, \tag{7}$$

where $\sigma=\sqrt{2T\gamma}$ and W is a standard Wiener process.

III. NUMERICAL METHODS

A common way to investigate the Langevin equation both by analytical and numerical methods consists in the reduction of it to the Fokker-Planck equation (FPE),[25] which is a deterministic partial differential equation for the distribution function $P(x,v,\tau)$. However, an analytical solution of the FPE for multiwell potentials has turned out to be possible only in the limiting cases when the temperature is much larger or much smaller than the height of the barrier between wells. As to a numerical solution of the FPE, difference schemes[26] and the matrix continued fraction method,[25] which allow one to calculate $P(x,v,\tau)$ effectively, were developed.

First of all we are interested in the power spectral density (PSD)

$$S(\omega)=\left|\int_{-\infty}^{+\infty}d\tau e^{i\omega\tau}[\langle x(\tau)x(0)\rangle-\overline{x^2}]\right|^2, \tag{8}$$

which is directly connected with the quantities observed in experiment. Here the angular brackets denote averaging over realizations of the stochastic process $x(\tau)$, and $\overline{x}$ is the stationary mean value. However, information on the behavior of individual trajectories is necessary for a reliable interpretation of the peculiarities and fine features of the PSD $S(\omega)$. Hence, more detailed information on the dynamics of the investigated system is required for us than is implied from the distribution function $P(x,v,\tau)$. That is why we use methods of numerical integration of SDE's (numerical experiment).

Thus we have to solve problems of two types. On the one hand, computation of individual trajectories requires one to apply methods that reproduce the dynamics of the investigated system sufficiently accurately for each realization of the stochastic process [so-called mean-square (strong) methods]. On the other hand, the strong methods are ''redundant'' to calculate mean values, such as $\langle x(\tau)x(0)\rangle$, and one can go over to weak methods which are simpler than the mean-square ones. The definitions and detailed discussion of the mean-square and weak methods were given in Refs. 21,22,27.

We used both Taylor-type and Runge-Kutta methods[21,22] as mean-square approximations. According to such features of the system of SDE's, Eqs. (7), such as the presence of stochastic terms only in the second equation, dispersion constancy (independent on time additive noise), linearity of the equations with respect to v, and independence of the right side of the first equation on x, the numerical schemes are strongly simplified even compared to methods for SDE's with additive noises.

The Taylor-type mean-square method of the third order for the SDE's, Eqs. (7), has the form[28]

$$x_{k+1}=x_k+hv_k-\frac{h^2}{2}[U'(x_k)+\gamma v_k]+\frac{h^3}{6}[-v_kU''(x_k)+\gamma(U'(x_k)+\gamma v_k)]+\sigma I_1-\gamma\sigma I_3,$$

$$v_{k+1}=v_k-h[U'(x_k)+\gamma v_k]+\frac{h^2}{2}[-v_kU''(x_k)+\gamma(U'(x_k)+\gamma v_k)]+\frac{h^3}{6}\{-v_k^2U'''(x_k)+\gamma v_kU''(x_k)-[U'(x_k)+\gamma v_k][\gamma^2-U''(x_k)]\}+\sigma I_1-\gamma\sigma I_2+[\gamma^2-U''(x_k)]\sigma I_3, \tag{9}$$

$$I_1=h^{1/2}\xi_k,\quad I_2=\frac{h^{3/2}}{2}\left(\frac{\eta_k}{\sqrt{3}}+\xi_k\right),$$

$$I_3=\frac{h^{5/2}}{2}\left(\frac{\xi_k}{3}+\frac{\eta_k}{2\sqrt{3}}-\frac{\zeta_k}{6\sqrt{5}}\right). \tag{10}$$

Here x_k and v_k are the mean-square approximations of the coordinate and the velocity at the instant of time τ_k, and $h=\tau_{k+1}-\tau_k$; ξ_k, η_k, and ζ_k are independently normally distributed variables with zero mean and unit variance.

The Runge-Kutta mean-square method of the second order for the system (7) takes the form[21]

$$x_{k+1}=x_k+\frac{h}{2}[v_k+\bar{v}_k]+\sigma\left(I_2-\frac{h}{2}I_1\right), \tag{11}$$

$$v_{k+1}=v_k-\frac{h}{2}\{[U'(x_k)+\gamma v_k]+[U'(\bar{x}_k)+\gamma \bar{v}_k]\}+\sigma I_1 - \gamma\sigma\left(I_2-\frac{h}{2}I_1\right),$$

$$\bar{x}_k=x_k+hv_k, \bar{v}_k=v_k-h[U'(x_k)+\gamma v_k]+\sigma I_1.$$

The notation is the same as in (9) and (10). Note that for the system (7) the mean-square method (11) contains only the first derivative of the potential and, hence, the scheme (11) is the fully Runge-Kutta method.

Due to the specific features of the SDE's, Eqs. (7), weak methods take the same forms as the corresponding mean-square approximations, but the quantities I_1, I_2, and I_3 can be simulated much more easily. For example, for the Taylor-type weak method of the third order we have[21]

$$I_1=h^{1/2}\xi_k, \quad I_2=\frac{h^{3/2}}{2}(\xi_k+2\eta_k), \quad I_3=h^{5/2}\left(\frac{\xi_k}{6}+\eta_k\right), \tag{12}$$

where the random variables ξ_k and η_k are distributed according to the law

$$\Pi(\xi=-1)=\Pi(\xi=1)=\frac{3}{10},$$

$$\Pi(\xi=-\sqrt{6})=\Pi(\xi=\sqrt{6})=\frac{1}{30},$$

$$\Pi(\xi=0)=\frac{1}{3}, \quad \Pi\left(\eta=-\frac{1}{\sqrt{12}}\right)=\Pi\left(\eta=\frac{1}{\sqrt{12}}\right)=\frac{1}{2}, \tag{13}$$

where $\Pi(\xi=a)$ is the probability of an event $\xi=a$.

In the case of the Runge-Kutta weak method of the second order, the quantities I_1 and I_2, are simulated as[21]

$$I_1=h^{1/2}\xi_k, \quad I_2=\frac{h}{2}I_1, \tag{14}$$

and the random variables ξ_k are distributed according to the law

$$\Pi(\xi=0)=\frac{2}{3}, \quad \Pi(\xi=-\sqrt{3})=\Pi(\xi=\sqrt{3})=\frac{1}{6}. \tag{15}$$

Thus, due to Ref. 21 it is sufficient to use a uniform distribution of random numbers for weak methods instead of the normal one as in the case of the mean-square approximations. This fact does explain the computational efficiency of the weak approximations for the SDE's, Eqs. (7).

At the end of the section we shall point out the problems arising during calculation of the PSD $S(\omega)$. There are three main difficulties.

(1) The integration interval, on which the SDE's, Eqs. (7) are solved, is finite.

(2) The function $\langle x(\tau)x(0)\rangle$ is calculated only in a discrete set of points.

(3) The correlator $\langle x(\tau)x(0)\rangle$ is computed with some numerical error. It is difficult to diminish this, since the Monte Carlo error is inversely proportional to the square root of a number of statistical tests (realizations).

The first problem leads to the following requirements concerning the interval length of integration of the system (7). The function $\langle x(\tau)x(0)\rangle$ has to achieve its stationary mean value and, at least, the length of the integration interval must not be less than a period of the slowest oscillations in the physical system.

To overcome the difficulties mentioned above we use the classical method of spectral estimation, namely, Welch's periodogram method with window (or tapering) functions of Hamming and Nuttall types.[29] Let us discuss the reasons which determine our choice of the concrete methods on the following example. Let a system with a discrete spectrum of frequencies ω_i exist. Actual calculations lead to a broadening of the peaks at $\omega=\omega_i$. In addition, sidelobes appear near these peaks. Then, if a peak at $\omega=\omega_1$ with large spectral weight and a peak at $\omega=\omega_2$ with much smaller spectral weight are close to each other, the last one can be ''hidden'' by the sidelobes of the main large peak. To get rid of the sidelobes the procedure of convolution with a so-called window (or tapering) function is used. But suppression of the sidelobes is always accompanied by a broadening of the main peaks. That is why the choice of that or another procedure of spectrum calculation depends on the concrete aims. Use of the Hamming window function gives lesser broadening of the peaks and, therefore, draws a spectrum with more details. In turn, use of the Nuttall window function allows us to suppress the sidelobes more effectively and, thus, gives a more adequate general picture of the spectrum.

In conclusion we note that, by virtue of the numerical error of the calculation of the function $\langle x(\tau)x(0)\rangle$, the values of the frequencies ω_i vary themselves with time. The influence of such nonphysical variations on $S(\omega)$ can be partially eliminated by division of numerical data into segments and further averaging of spectrum over the segments.

IV. NUMERICAL RESULTS

A. Bistable potential

The potential shown in Fig. 2 (dashed line) is approximated by the analytical expression

$$V(x)=\overline{\alpha}x^2+\overline{\beta}x^4, \quad \overline{\alpha}=-0.6 \text{ (Ry/atom)}, \quad \overline{\beta}=30 \text{ (Ry/atom)} \tag{16}$$

according to Ref. 7.

The Taylor-type method of the third order (9) was used for calculation of realizations $x(\tau)$. As a rule, the step of integration was chosen equal to 0.1. In this case the error of numerical integration of SDE's was of the same order as the Monte Carlo one with averaging over realizations ($\sim N^{1/2}$, where N is the number of realizations, in our calculations $N=10^5$). The additional numerical investigations with variation of the integration step size confirmed the validity of the selected values. The parameter γ in Eq. (5), which we identified as a phonon damping, was equal to $\gamma=0.065$ compared to the order of typical values of the damping in metals.[30] The temperature T was measured in the barrier heights $\Delta E=470$ K. We chose the initial conditions as

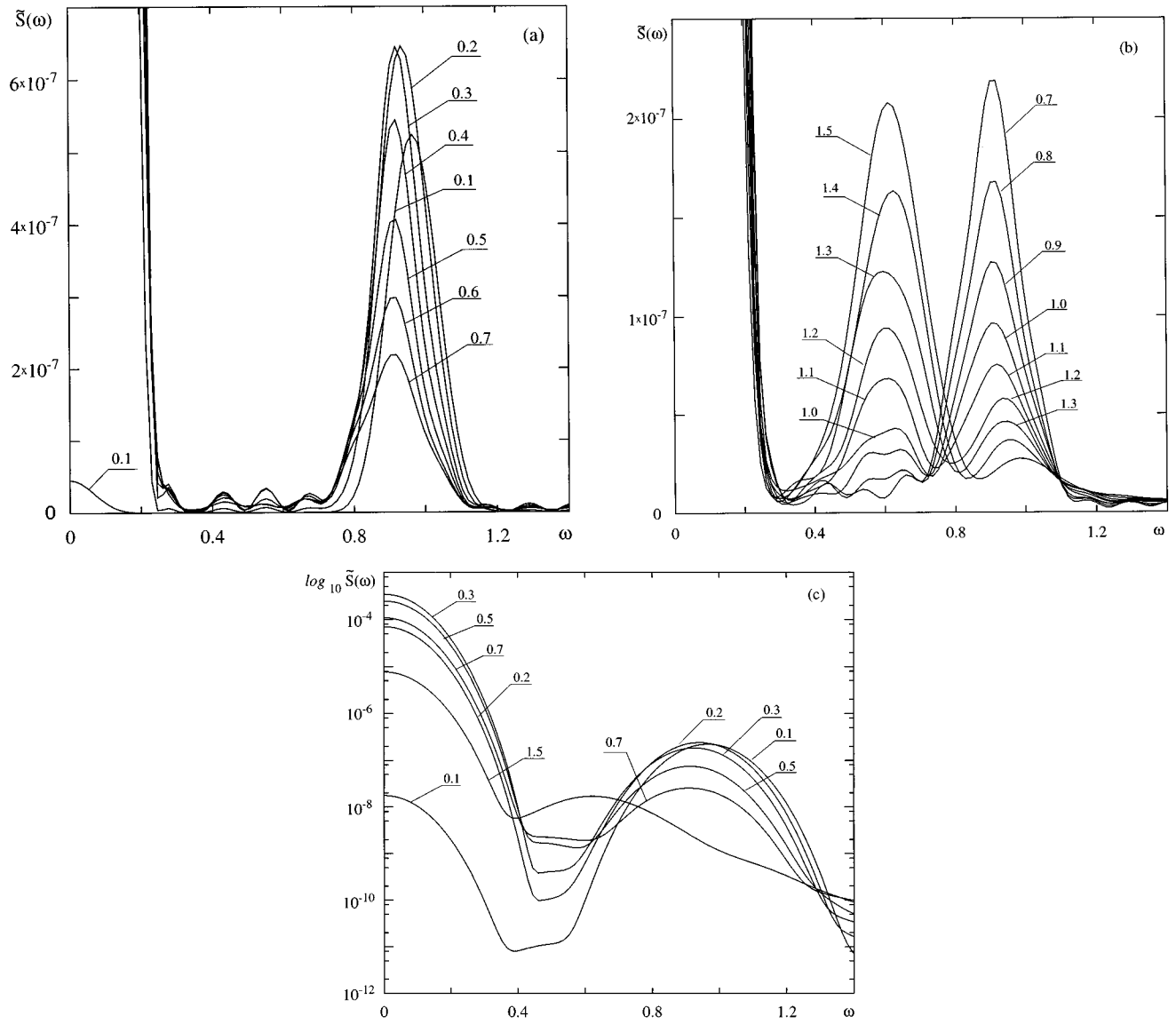

FIG. 3. PSD $\tilde{S}(\omega)=S(\omega)/x^2(0)$ for the anharmonic oscillator in the bistable potential in the temperature range from 0.1 to 0.7 (a), from 0.7 to 1.5 (b), and in semilogarithmic scale (c). The temperature is in barrier height units. Averaging was carried out over 10^5 realizations containing 5000 points with an integration step 0.1. The length of the segments during the spectral estimation was equal to 512 points. The Hamming (a), (b) and Nuttall (c) windows and half overlapping of segments were chosen.

$x(0)=\sqrt{\alpha/2\beta},\ v(0)=\sqrt{T}$; i.e., the particle was considered to be at the bottom of one of the wells with the thermal velocity at $\tau=0$.

The results for $S(\omega)$ are presented for various temperatures in Fig. 3. For $T\ll 1$ [Fig. 3(a)] the peak at $\omega\approx 1$, which is caused by small oscillations near the well's bottom, dominates in $S(\omega)$. One can see that while the temperature is increasing this peak shifts to lower frequencies by virtue of the dependence of the frequency on the oscillation amplitude caused by anharmonicities. At $T=0.2$ the central peak appears in $S(\omega)$ [see Fig. 3(c), in which PSD $S(\omega)$ is plotted in semilogarithmic scale]. In a narrow interval of temperature close to $T\approx 1$ the PSD shape is changed once more; namely, the maximum at $\omega\approx 0.5$ appears. Moreover, most of the spectral density is concentrated in this peak while the peak at $\omega\approx 1$ is disappearing [Fig. 3(b)].

To understand the reasons for such behavior of the PSD $S(\omega)$ a typical trajectory at $T\approx 0.5$ is presented in Fig. 4. The processes of three types are clearly visible: (i) oscillations in one of the wells (fast oscillations) and (ii) transitions between wells of the two types: (a) transitions with trapping in the second well and (b) transitions with immediate return to the first well.

In Fig. 4 these processes are marked by the labels I, II, and III. The processes of the second and third types we shall call as trapped transitions and transitions with return, correspondingly. The last ones were called ''flight trajectories'' in Ref. 13.

Essentially the transitions with return can be considered as oscillations covering the two wells. The period of such oscillations may be roughly estimated as a doubled period of oscillations in one well. Thus, it is natural to suggest that the middle peak in $S(\omega)$ (at $\omega\approx 0.5$) is connected with such a process. As to the central peak, it is natural to associate it with the slowest process of the second type. If transitions from one well to another happened with just the same semi-

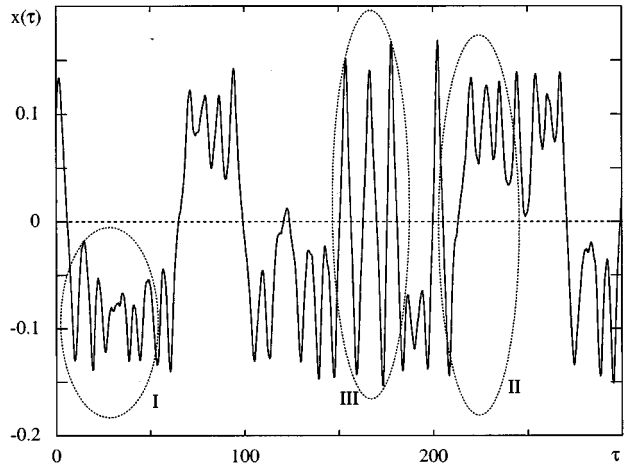

FIG. 4. A typical trajectory of the anharmonic oscillator in the bistable potential ($T=0.8$, $\gamma=0.065$, *and* h$=0.001$). The labels I, II, and III mark typical processes (see text of the paper).

period t_1 (the first exit time), then the central peak would be situated at the frequency $\omega_1=\pi/t_1$. Actually, the first exit time t_1 is a random variable and the shape of the central peak is determined by its distribution function $F(t_1)$. This function is shown in Fig. 5 for a certain value of temperature. One can see that the dispersion of t_1 has the order of the mean value of the first exit time t_1 which, in turn, does not correspond to the maximum of $F(t_1)$ (see Fig. 5). Precisely this circumstance leads to the maximum near $\omega=0$ in $S(\omega)$. The large height of the peak is caused by the large amplitude of transitions between wells compared to that of oscillations in each well.

The following procedure proves directly that the central peak is caused by the trapped transition processes. These processes can be removed by the replacement of $x(\tau)$ to

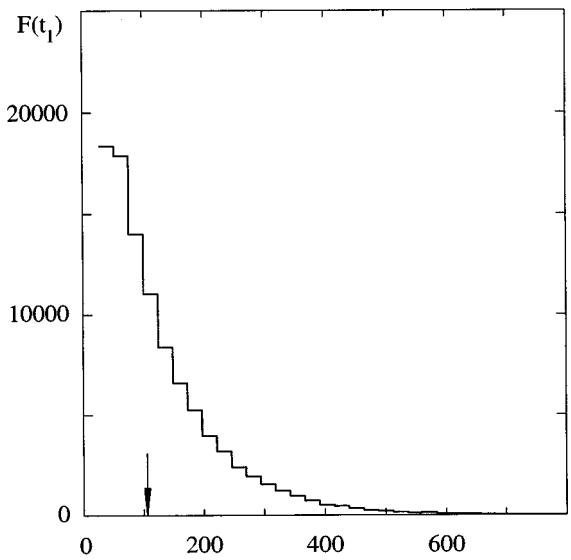

FIG. 5. The distribution function of the first exit time at $T=0.5$. Averaging was carried out over 10^5 trajectories with an integration step 0.1. The arrow marks the mean of the first exit times.

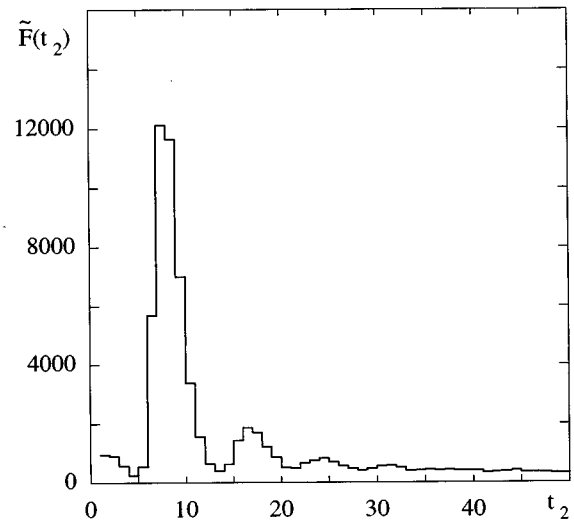

FIG. 6. The distribution function of the second exit time at $T=0.5$. Averaging was carried out over 10^5 trajectories with an integration step 0.1.

$|x(\tau)|$ in the PSD $S(\omega)$, which imitates the merging of the two wells. The central peak practically disappears when this replacement is done.

To investigate the contribution of the transitions with return it is useful to introduce a distribution function $\tilde{F}(t_2)$ of the second exit time t_2. This quantity is determined in the following way. Let the position of the oscillator at the bottom of the well be the initial one. Then the time t_2 is defined as an interval between the first and the second appearances of an oscillator at the barrier's position. The distribution function $\tilde{F}(t_2)$ is shown for a certain temperature in Fig. 6. In contrast to the distribution function $F(t_1)$, it has a sharp peak just at $t_2\approx\pi/\omega_{\text{left}}$ where $\omega_{\text{left}}\approx 0.5$ is the frequency of the processes of the third type. The height of the middle peak in $S(\omega)$ is less than that of the central one because the probability of such processes is very small. At last, if we simply remove parts corresponding to the processes of type III from the trajectories, then the middle maximum disappears in $S(\omega)$.

B. Three-well potential

Consider the case of the potential $V(x)$ which is shown by the solid line in Fig. 2. In contrast to the previous case, the potential was given in tabular form and is approximated by cubic splines. To avoid calculation of the higher derivatives of $V(x)$ used in the Taylor-type method [see (9)] we applied the Runge-Kutta method of the second order [see (11)]. The initial conditions were chosen in the form $x(0)=x_0$ (center of the deepest well), $v(0)=\sqrt{T}$. The temperature is measured in the heights of the barrier $\Delta E_1=72$ K counted from the bottom of the shallow well (barrier height measured from the bottom of the deepest well is $\Delta E_2\approx 8\Delta E_1$).

The results of calculations for $S(\omega)$ and $x(\tau)$ are presented in Figs. 7 and 8. The principal qualitative difference from the previous case consists in the absence of the central peak. This is explained by the fact that the oscillator gets trapped by the shallow well with a small probability because the condition $\Delta E_1 \ll \Delta E_2$ holds.

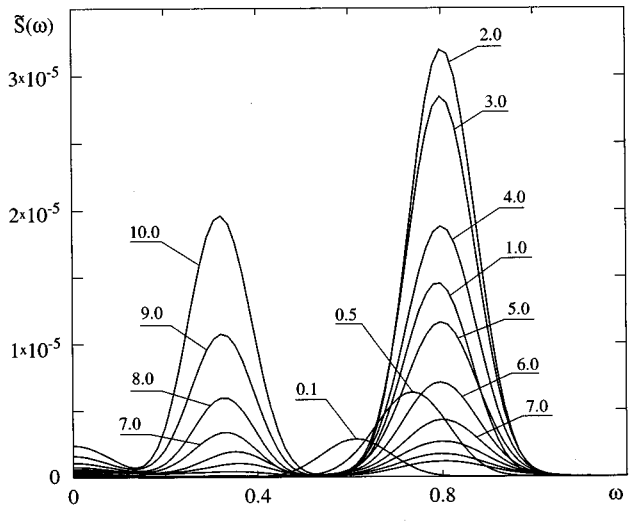

FIG. 7. PSD $\tilde{S}(\omega)=S(\omega)/x^2(0)$ for the anharmonic oscillator in the three-well potential in the temperature range from 0.1 to 10.0 (the temperature is in barrier height units). Averaging was carried out over 10^5 realizations containing 5000 points with an integration step 0.1. The length of the segments during the spectral estimation was equal to 512 points. The Hamming window and half overlapping of segments were chosen.

We can point out the processes of the four types with their typical frequencies: Label I denotes oscillations in the deep well, oscillations in one of the shallow wells are marked by label II, label III denotes the processes of transitions from a deep well to a shallow one with return, and the transitions from one shallow well to another with return are marked by label IV. The typical frequencies of the processes, labeled by III and IV, are very close to each other and determine the low-frequency maximum of $S(\omega)$ (at $\omega\approx 0.5$); at the same time the high-frequency peak is practically completely determined by processes of the first type (processes of the second type have both small probability and small amplitude of oscillations). Note that while the temperature is increasing, the high-frequency maximum shifts to higher frequencies on account of anharmonic effects in contrast to the case of the bistable potential. This shift is the most noticeable in the temperature range from 0.1 to 2. Thus, the low-frequency peak is caused by oscillations covering all three wells and the high-frequency one is determined by oscillations in the deep well. We notice that the heights of the peaks are equal at $T\approx\Delta E_2$.

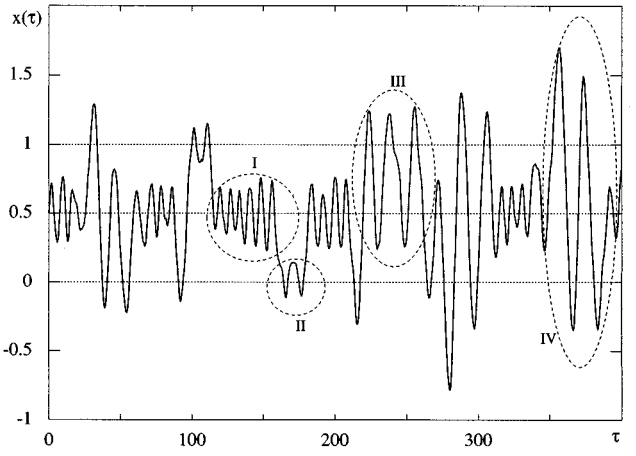

FIG. 8. A typical trajectory of the anharmonic oscillator in the three-well potential ($T=6.0$, $\gamma=0.065$, *and* $h=0.1$). The labels I, II, III, and IV mark typical processes (see text of the paper).

V. DISCUSSION OF RESULTS

One should stress three most important circumstances.

(I) If the model investigated in the present paper is considered as a certain simplified description of lattice dynamics for realistic systems above the structural transition temperature, then the appearance of the additional peak in $S(\omega)$ at intermediate frequencies seems to be very unusual. These frequencies [see Fig. 3(b) and Fig. 7] are smaller than those typical for oscillations in a well, but essentially greater than those typical for the central peak. Indeed, let us suppose that in inelastic neutron scattering experiments the distribution in transferred energy, like that represented in Fig. 3(b) and Fig. 7, is observed when the transferred momentum $\mathbf{Q}$ and the polarization vector $\mathbf{e}_\nu$ are fixed. In the usual situation the PSD $S(\omega)$ can have only one maximum, the position of which corresponds to the phonon frequency $\omega_\nu(\mathbf{Q})$. If two maxima are observed, then they could be interpreted as a splitting of the phonon branch into two ones. However, the detailed analysis of origin of the second peak in $S(\omega)$ (at the intermediate frequency), which is presented in the previous section, shows that it is caused by processes having little to do with ''naive'' ideas about atom vibrations in the phonon picture (transitions with return). Just in this sense we speak about the inadequacy of the phonon picture for such situations. Otherwise, if at the initial instant of time a spatial distribution of the atom displacement field is given in the form $\cos(\mathbf{Q}\cdot\mathbf{R})$ (when the spatial dispersion is absent it remains just the same at any instant of time), then its time dependence has nothing resembling the simple damped oscillations of the form $\cos(\mathbf{Q}\cdot\mathbf{R}-\omega_{\mathbf{Q}}t)\exp(-\gamma_{\mathbf{Q}}t)$. Perhaps, just that very circumstance is the cause of the appearance of the symmetrically forbidden splitting of branches in Zr-Nb[2] alloys, which is accompanied by a considerable broadening of the peaks. Of course, the spatial dispersion plays an important part in the actual situation, since the anomalous behavior of phonons takes place in a sufficiently large area of the wave vector space.[2]

(II) The next important circumstance is the following. Starting from traditional ideas, intensity swapping in $S(\omega)$ from the right peak to the left one can be considered as an unusually strong dependence of the phonon frequency on temperature. Really, as we have seen, the situation is essentially more complicated.

(III) Now let us pass to a discussion of the central peak. In the model considered it is caused by trapped processes and appears only in the case of symmetrical wells. It is natural to assume that if the difference between the well depths is not too large, such a peak also exists; anyway it is absent when $\Delta E_2\gg\Delta E_1$ (see Sec. IV B). The central peak has noticeable intensity (for the model analyzed in Sec. IV A) at $0.2\Delta E\leqslant T\leqslant\Delta E$ with the maximal intensity at $T=0.3\Delta E$; see Fig. 3(c). These results can possibly explain, as discussed in Ref. 1, the difference between alloys of Ti and Zr in the

$\beta+\omega$ phase, where the central peak is clearly observed, and the β phase of pure Ti and Zr near the melting temperature, where a wideband distribution was observed in $S(\omega)$ without a clearly visible central peak. This difference can be associated with either the larger closeness of the depths of the wells corresponding to the β and ω phases in alloys or to different ratio between ΔE and T in these two cases. Let us recall once more that at high temperatures the potential $V(X)$ for β-Zr differs from that shown in Fig. 2 since it is necessary to take into account the entropy contribution. Thus the comparison with experiments can be only qualitative. We also note that the central peak in Zr-Nb alloys is observed in the same region of the wave vector space where the splitting of the phonon branches occurs,[2] which does not contradict the considered model of the symmetric wells. For the sharply asymmetric case (see Fig. 7) the splitting can take place without the central peak. The results conform the kink theory of the central peak[4] in the sense that a kink of the type considered in Ref. 4 exists only in the case of symmetrical wells (bistable potential).

Despite the model under consideration being not quite realistic and, therefore, the results obtained here being not conclusive (e.g., due to neglect of the entropy contribution to the effective potential), the main features of the dynamic structure factor observed in Ref. 1 may be explained qualitatively even in this simple approach. In our opinion, this explanation is possible due to the small sensitivity of these rough features to the details of the shape of potential curves.

It is worthwhile to note in conclusion that the results of the simulations presented here may be applied to situations which are quite different from lattice vibrations, due to the importance of the concept of a multiwell potential in a very broad field of phenomena. As an example one can compare the results of our simulations (see Fig. 4) with the experimental data on stochastic resonance in paramagnetic resonance systems.[31]

ACKNOWLEDGMENTS

We would like to thank Dr. M. V. Tret'yakov for many helpful discussions and generously providing us with unpublished results concerning the numerical methods of Langevin equation integration. This work has been supported by the International Science Foundation under Grant No. RGQ300 and the Russian Basic Research Foundation under Grant No. 95-02-06426.

*Electronic address: Serghey.Tretjakov@usu.ru

[1] W. Petry, Phase Trans. B **31**, 119 (1991); J. Phys. (Paris) Colloq. **5**, 2-15 (1995).

[2] J.D. Axe, D.T. Keating, and S.C. Moss, Phys. Rev. Lett. **35**, 530 (1975).

[3] W. Lin, H. Spalt, and B.W. Batterman, Phys. Rev. B **13**, 5158 (1976).

[4] J.A. Krumhansl and J.R. Schrieffer, Phys. Rev. B **11**, 3535 (1975).

[5] M.I. Katsnelson and A.V. Trefilov, Fiz. Met. Metalloved. **64**, 629 (1987) [Phys. Met. Mellallogr. (USSR) **64**(4), 1 (1987)].

[6] K.-M. Ho, C.L. Fu, and B.N. Harmon, Phys. Rev. B **29**, 1575 (1984).

[7] Y.-Y. Ye *et al.*, Phys. Rev. Lett. **58**, 1769 (1987).

[8] Y. Chen, K.-M. Ho, and B.N. Harmon, Phys. Rev. B **37**, 283 (1988).

[9] Phase Transit. B **49**, (1994).

[10] H. Böttger, *Principles of the Theory of Lattice Dynamics* (Academic-Verlag, Berlin, 1983).

[11] R.J. Gooding and J.A. Krumhansl, Phys. Rev. B **38**, 1695 (1988); **39**, 1535 (1989); G.R. Barsch and J.A. Krumhansl, Metall. Trans. A **19**, 761 (1988).

[12] V.V. Kiseliev, Phys. Lett. A **196**, 97 (1994).

[13] Y.N. Gornostyrev, M.I. Katsnelson, and A.V. Trefilov, Pis'ma Zh. Éksp. Theor. Fiz. **56**, 542 (1992) [JETP Lett. **56**, 529 (1996)].

[14] J.R. Morris and R.J. Gooding, Phys. Rev. B **46**, 8733 (1992).

[15] V.G. Vaks, *Introduction to Microscopic Theory of Ferroelectrics* (Nauka, Moscow, 1973).

[16] M.I. Katsnelson and A.V. Trefilov, Zh. Éksp. Theor. Fiz. **97**, 1892 (1990) [Sov. Phys. JETP **70**, 1067 (1996)].

[17] N.N. Bogoliubov, *Collection of Papers* (Naukova Dumka, Kiev, 1970), Vol. 2, pp. 77–98.

[18] N.G. Van Kampen, *Stochastic Processes in Physics and Chemistry* (North-Holland, Amsterdam, 1984); C.W. Gardiner, *Handbook of Stochastic Methods* (Springer-Verlag, Berlin, 1985).

[19] U. Eckern, W. Lehr, A. Menzel-Dorwarth, F. Pelzer, and A. Schmid, J. Stat. Phys. **59**, 885 (1990).

[20] T. Schneider and E. Stoll, Phys. Rev. B **17**, 1302 (1978).

[21] G.N. Milstein, *Numerical Integration of Stochastic Differential Equations* (Kluwer Academic, Dordrecht, 1995).

[22] P.E. Kloeden and E. Platen, *Numerical Solution of Stochastic Differential Equations* (Springer-Verlag, Berlin, 1992).

[23] S. Nosé, Prog. Theor. Phys. Suppl. **3**, 46 (1991).

[24] B.L. Holian, H.A. Posch, and W.G. Hoover, Phys. Rev. A **42**, 3196 (1990).

[25] H. Risken, *The Fokker-Planck Equation* (Springer-Verlag, Berlin, 1984).

[26] V. Palleschi, F. Sarri, G. Marcozzi, and M.R. Forquati, Phys. Lett. A **146**, 378 (1990).

[27] G.N. Milshtein, Theor. Prob. Appl. **19**, 557 (1974); **23**, 396 (1978).

[28] M.V. Tret'yakov (private communication). [The Taylor-type method of the third order used in the present paper was obtained by the expansion of the exact solution of the SDE's, Eqs. (7), over Itô integrals. Such procedure is called the Wagner-Platen expansion Refs. 21 and 22 and is a stochastic analog of the deterministic Taylor series.]

[29] S.L. Marple, Jr., *Digital Spectral Analysis* (Prentice-Hall, Englewood Cliffs, NJ, 1987).

[30] V.G. Vaks, S.P. Kravchuk, and A.V. Trefilov, J. Phys. F **10**, 2105 (1980).

[31] L. Grammaitoni, M. Martinelli, L. Pardi, and S. Santucci, J. Stat. Phys. **70**, 425 (1993).